2-1-2000

Disorder-Induced Desynchronization in a 2x2 Circular Josephson Junction Array

Adam S. Landsberg
Claremont McKenna College; Pitzer College; Scripps College

Recommended Citation

Landsberg, A.S. "Disorder-induced Desynchronization in a 2x2 Circular Josephson Junction Array." Physical Review B 61.5 (2000): 3641-3648. DOI: 10.1103/PhysRevB.61.3641

Disorder-induced desynchronization in a 2×2 circular Josephson junction array

A. S. Landsberg
W. M. Keck Science Center, The Claremont Colleges, Claremont, California 91711
(Received 16 August 1999)

Analytical results are presented which characterize the behavior of a dc-biased, two-dimensional circular array of overdamped Josephson junctions subject to increasing levels of disorder. It is shown that high levels of disorder can abruptly destroy the synchronous functioning of the array. We identify the transition boundary between synchronized and desynchronized behavior, along with the mechanism responsible for the loss of frequency locking. Comparisons with recent results for arrays with rectangular lattice geometries are described.

I. INTRODUCTION

Josephson junction arrays, comprised of multiple Josephson junctions coupled to one another, offer many potential benefits over solitary junctions in terms of possible device applications (e.g., Refs. 1–5). Since many common array applications require that the junctions oscillate in a coherent manner, a key design goal is determining which array types are most amenable to supporting a synchronous mode of operation. Achieving this goal is complicated, however, by the presence of disorder in an array (i.e., small variations in the individual junction characteristics), which is unavoidably introduced during the manufacturing process. Such nonuniformities can potentially disrupt the coherent functioning of the array. For this reason, understanding and designing against the desynchronizing effects of disorder represents an important yet challenging consideration in array design.

At present, a number of different ways of promoting coherent oscillations in arrays with disorder have been identified. Some involve linking the array in an external fashion (e.g., coupling the array to an external load, applying a high-frequency external signal, etc.), while others rely on various spatially distributed array designs that demand a somewhat more sophisticated analysis to properly model (since the standard ''lump circuit'' analysis fails).[6–8] Though these approaches can at times be effective, a basic underlying question remains largely unanswered: To what extent does the *lattice geometry* of an array determine its intrinsic robustness against disorder? In particular, are certain array geometries naturally more conducive to maintaining coherence in the presence of disorder than others?

While we cannot fully address this larger question, our intention in this paper is to garner some modest insight into this problem by examining the behavior of one particular geometric model (a ''circular plaquette''). This model represents the simplest possible (nontrivial) two-dimensional circular array, and our aim is to provide a detailed description of how disorder affects this system's synchronization properties. Since our larger objective is to isolate the influence of lattice geometry on behavior, our model array is highly stripped down, i.e., the circular plaquette is a ''bare'' array which is entirely free of external loads, signals, and spatial-distribution effects like those described above which might otherwise obscure the intrinsic contribution of lattice geometry to the overall synchronization process. For this same reason, we choose to model the individual junctions making up the array in the simplest possible fashion, i.e., we use the resistively shunted junction (RSJ) model.[2] Although our circular plaquette model is admittedly quite special, we hope that it might serve as a prototype and that a number of key results which come out of our study will prove useful more generally for studies of other lattice geometries. Specifically, we will identify the principle physical mechanism responsible for (disorder-induced) desynchronization in this system, and also analytically construct the transition boundary separating sychronized from desynchronized behavior by employing a useful perturbative approach.

Our focus on the two-dimensional circular-lattice structure of the plaquette model is motivated by twin considerations: First, recent work suggests that two-dimensional array designs might enjoy a significant advantage over their one-dimensional counterparts in their ability to maintain coherence in the presence of disorder.[9–15] Second, studies of prototype two-dimensional arrays with a rectangular lattice geometry have recently yielded analytic estimations of their ability to tolerate disorder.[14,15] Thus, a detailed analysis of an array with circular geometry will permit a direct comparison of the relative merits of these two types of lattice geometries.

This paper is organized as follows. In Sec. II we describe the basic circular plaquette model and construct the equations of motion. Section III presents a formal asymptotic analysis leading to the construction of the transition boundary separating synchronized from desynchronized behavior as a function of disorder. Our theoretical predictions are then compared with results from numerical simulations. In Sec. IV we make a direct comparison between 2×2 arrays with circular and rectangular geometries, and then discuss generalizations to larger circular arrays as well as limitations of our model. Section V summarizes our main findings.

II. THE CIRCULAR PLAQUETTE: BASIC MODEL AND NUMERICAL BEHAVIOR

The circular plaquette model represents a 2×2 array consisting of six overdamped [i.e., RSJ (Ref. 2)] Josephson junctions. A dc bias current I is fed in uniformly from the outside

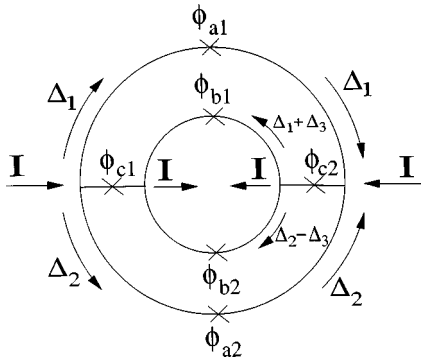

FIG. 1. *The circular plaquette.* The crosses mark the locations of the six junctions. Here, $\phi_{a1},\phi_{a2},\phi_{b1},\phi_{b2}$ are the phase differences across the four azimuthal junctions and ϕ_{c1},ϕ_{c2} denote the phase differences across the two radial junctions. I represents the (imposed) bias current, and $\Delta_1,\Delta_2,\Delta_3$ the (spontaneously induced) shunt currents.

and extracted uniformly along the inner edge, as shown in Fig. 1. The governing equations for the array follow from the dual constraints of current conservation and flux quantization. Letting $\Delta_1,\Delta_2,\Delta_3$ denote the spontaneously induced shunt currents in the array, the requirements of current conservation together with the fundamental Josephson relations yield the basic equations of motion

$$\frac{\hbar}{2er}\dot{\phi}_{c1}+I_{c1}\sin(\phi_{c1})=I-\Delta_1-\Delta_2, \tag{1a}$$

$$\frac{\hbar}{2er}\dot{\phi}_{c2}+I_{c2}\sin(\phi_{c2})=I+\Delta_1+\Delta_2, \tag{1b}$$

$$\frac{\hbar}{2er}\dot{\phi}_{a1}+I_{a1}\sin(\phi_{a1})=\Delta_1, \tag{1c}$$

$$\frac{\hbar}{2er}\dot{\phi}_{a2}+I_{a2}\sin(\phi_{a2})=\Delta_2, \tag{1d}$$

$$\frac{\hbar}{2er}\dot{\phi}_{b1}+I_{b1}\sin(\phi_{b1})=\Delta_1+\Delta_3, \tag{1e}$$

$$\frac{\hbar}{2er}\dot{\phi}_{b2}+I_{b2}\sin(\phi_{b2})=\Delta_2-\Delta_3, \tag{1f}$$

where the ϕ's denote the phase differences across the various junctions. Disorder has been included in the model by allowing the critical currents of the six junctions $(I_{c1},I_{c2},I_{a1},I_{a2},I_{b1},I_{b2})$ to be nonidentical. (Note, however, that we neglect disorder in the junction resistances r here, in keeping with most prior studies; see Ref. 15 for a discussion of this issue.)

The above equations must be supplemented by the additional constraints imposed by flux quantization. In particular, in the absence of magnetic fields, the sum of the phase differences around any closed loop must be zero. This yields

$$\phi_{a1}-\phi_{a2}=0,\quad \phi_{b1}-\phi_{b2}=0,\quad \phi_{a1}+\phi_{c2}+\phi_{b1}-\phi_{c1}=0. \tag{2}$$

Together, Eqs. (1a)–(1f), (2) constitute our basic model.

An inspection of these governing equations reveals that, in the absence of disorder, there exists a synchronized solution in which the two radial junctions oscillate in perfect synchrony $[\phi_{c1}(t)=\phi_{c2}(t)]$, while the azimuthal junctions are completely inactive $[\phi_{a1}(t)=\phi_{a2}(t)=\phi_{b1}(t)=\phi_{b2}(t)=0]$. This solution, known as the ''in-phase state,'' is dynamically stable when no disorder is present, as a straightforward stability analysis reveals. For many potential device applications involving Josephson junction arrays, the in-phase state—a state of perfect synchrony—represents the ideal operating state of the system.

Our main interest in this paper, however, is in the behavior of the system when disorder is present. A numerical survey of our model for different realizations of the disorder (obtained by varying the values of the critical currents $I_{c1},I_{c2},I_{a1},I_{a2},I_{b1},I_{b2}$) shows that there exist two general categories of solutions.

(a) *Synchronized states*. Here, the two radial junctions overturn at the same average rate: $\langle d\phi_{c1}/dt\rangle=\langle d\phi_{c2}/dt\rangle$. Meanwhile, the azimuthal junctions are active, but do not overturn: $\langle d\phi_{a1}/dt\rangle=\langle d\phi_{a2}/dt\rangle=\langle d\phi_{b1}/dt\rangle=\langle d\phi_{b2}/dt\rangle=0$. (The brackets $\langle\ \rangle$ denote time averages.) Figure 2 depicts a representative example of a synchronized state.

(b) *Desynchronized states*. In such states, the coherence between the two radial junctions is lost: $\langle d\phi_{c1}/dt\rangle\neq\langle d\phi_{c2}/dt\rangle$. The azimuthal junctions now overturn (i.e., their time averages are no longer zero). Figure 3 illustrates this loss of synchronization in the radial junctions.

For a fixed value of the bias current I, one observes that the array enters a synchronized state when the disorder is relatively low, while for high levels of disorder a desynchronized state is realized. If instead one fixes the level of disorder and varies the bias current, one finds synchronized behavior for high values of the bias current and desynchronized behavior for low values of the bias current. The transition between these two states is abrupt, as can be seen from the I-V plot depicted in Fig. 4.

Our objective is to explain these qualitative numerical observations and to construct an analytical characterization of the transition from synchronized to desynchronized behavior. We describe in the next section how this can be achieved through an asymptotic (multiple-time scale) analysis.

III. ANALYSIS OF THE PLAQUETTE

To proceed, we must first put Eqs. (1a)–(1f), (2) into a form more suitable for analysis. We begin by noting that while Eqs. (1a)–(1f) represents a six-dimensional system of equations (one for each of the six junctions), the presence of three constraint relations (2) implies that there are in fact only three dynamically independent phases in the problem. We arbitrarily choose $\phi_{c1},\phi_{c2},\phi_A$ as the three independent variables, where we have defined $\phi_A\equiv\phi_{a1}=\phi_{a2}$.

Next, we nondimensionalize the equations by rescaling time $[t\rightarrow(\hbar/2erI)t]$ and introduce dimensionless critical currents

$$i_{c1}=I_{c1}/I,\quad i_{c2}=I_{c2}/I,\quad i_A=\frac{I_{a1}+I_{a2}}{2I},\quad i_B=\frac{I_{b1}+I_{b2}}{2I}. \tag{3}$$

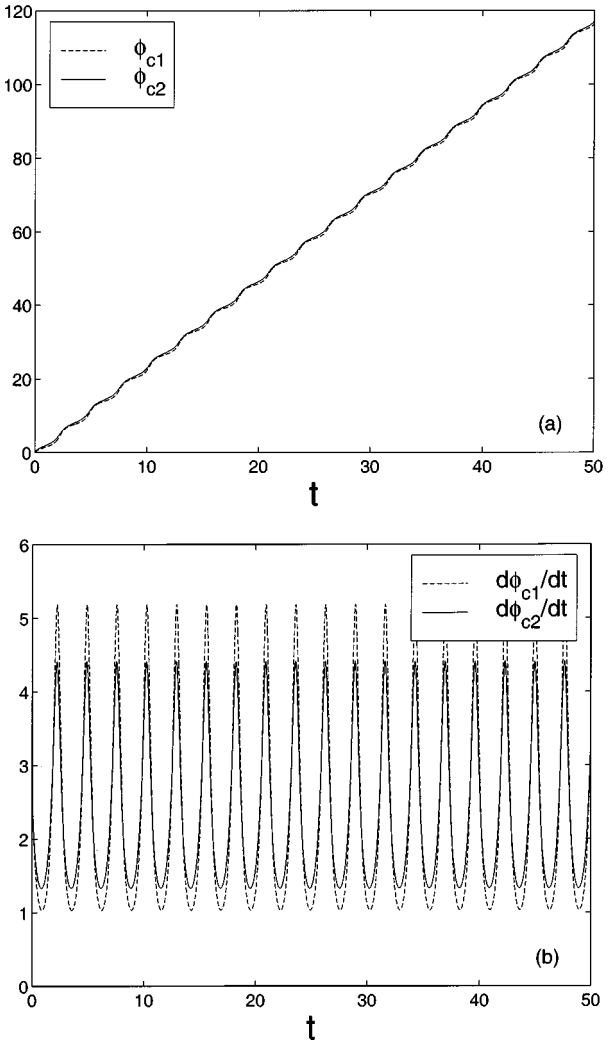

FIG. 2. (a) A synchronized state (for $I=3.0$, $I_{c1}=2.6$, $I_{c2}=1.1$, $I_{a1}=0.9$, $I_{a2}=0.7$, $I_{b1}=0.6$, $I_{b2}=0.8$). The phases of the two radial junctions ϕ_{c1},ϕ_{c2} are shown as a function of time. In the plot, the curves for ϕ_{c1} (dashed line) and ϕ_{c1} (solid line) are virtually indistinguishable, consistent with the fact that these two junctions grow at the same average rate [compare to Fig. 3(a)]. (b) The corresponding voltage oscillations across the radial junctions $(d\phi_{c1}/dt,\ d\phi_{c2}/dt)$. Note here that the instantaneous voltages have been plotted, rather than the time-averaged voltages, to better accentuate the frequency-locked nature of the synchronized state.

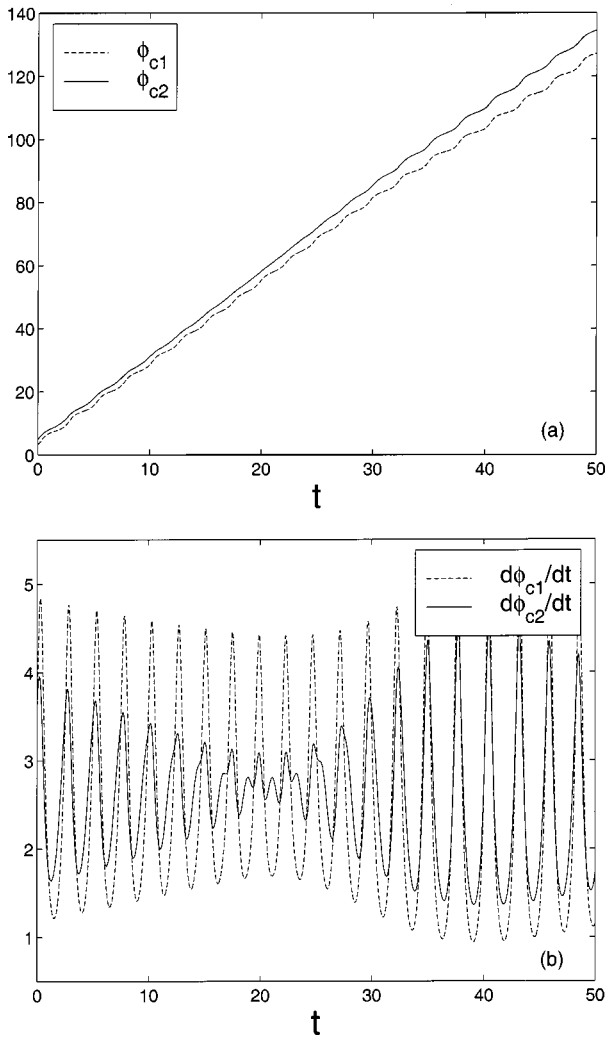

FIG. 3. (a) A desynchronized state (for $I=3.0$, $I_{c1}=2.6$, $I_{c2}=1.1$, $I_{a1}=0.1$, $I_{a2}=0.05$, $I_{b1}=0.2$, $I_{b2}=0.8$). Note that the two radial junctions (dashed curve ϕ_{c1}, solid curve ϕ_{c2}) have different average growth rates. (b) The corresponding voltage oscillations across the radial junctions $(d\phi_{c1}/dt,\ d\phi_{c2}/dt)$, illustrating the lack of coherent oscillations in the desynchronized state.

Note that this procedure has the effect of normalizing the bias current I to unity, so that the (dimensionless) critical currents (i_{c1},i_{c2},i_A,i_B) become small as the bias current becomes large. This will prove useful for our asymptotic analysis, which will focus on the high bias current regime, since the critical currents can then be treated as small parameters.

In dimensionless form, the equations for the circular plaquette become

$$\frac{d\phi_A}{dt}=-\frac{5}{6}i_A\sin(\phi_A)+\frac{1}{6}i_B\sin(\phi_{c1}-\phi_{c2}-\phi_A)+\frac{1}{6}i_{c2}\sin(\phi_{c2})-\frac{1}{6}i_{c1}\sin(\phi_{c1}), \tag{4a}$$

$$\frac{d\phi_{c1}}{dt}=1-\frac{1}{3}i_A\sin(\phi_A)-\frac{1}{3}i_B\sin(\phi_{c1}-\phi_{c2}-\phi_A)-\frac{1}{3}i_{c2}\sin(\phi_{c2})-\frac{2}{3}i_{c1}\sin(\phi_{c1}), \tag{4b}$$

$$\frac{d\phi_{c2}}{dt}=1+\frac{1}{3}i_A\sin(\phi_A)+\frac{1}{3}i_B\sin(\phi_{c1}-\phi_{c2}-\phi_A)-\frac{2}{3}i_{c2}\sin(\phi_{c2})-\frac{1}{3}i_{c1}\sin(\phi_{c1}). \tag{4c}$$

[Note here that the constraint relations (2) have been used to eliminate three of the six phases in Eqs. (1a)–(1f) and to reexpress the shunt currents $\Delta_1,\Delta_2,\Delta_3$ in terms of the three independent phases.]

One final manipulation is needed to prepare the system for analysis. We introduce new coordinates

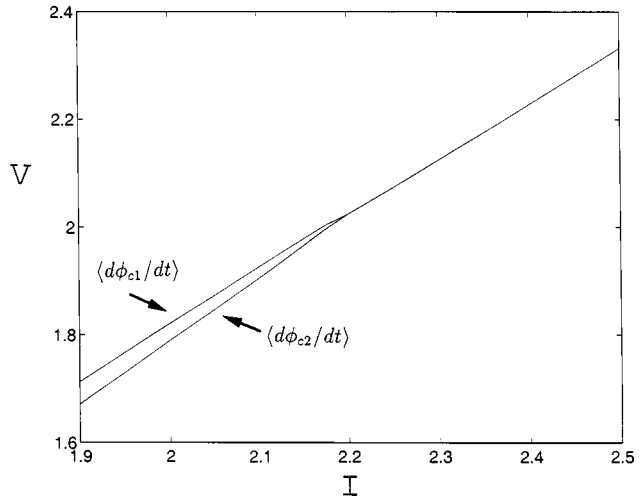

FIG. 4. *I-V* plot for the circular plaquette. The time-averaged voltage across each radial junction $\langle d\phi_{c1}/dt\rangle$, $\langle d\phi_{c2}/dt\rangle$ as a function of imposed current I is shown. The transition from a desynchronized to synchronized state near $I=2.2$ is clearly seen. (Here, $I_{c1}=0.3$, $I_{c2}=1.5$, $I_{a1}=0.06$, $I_{a2}=0.11$, $I_{b1}=0.4$, $I_{b2}=0.2$.)

$$\phi_C=\frac{\phi_{c1}+\phi_{c2}}{2},\quad \phi_{\Delta C}=\frac{\phi_{c1}-\phi_{c2}}{2}, \tag{5}$$

yielding

$$\frac{d\phi_A}{dt}=-\frac{5}{6}i_A\sin(\phi_A)+\frac{1}{6}i_B\sin(2\phi_{\Delta C}-\phi_A)+\frac{1}{6}i_{c2}\sin(\phi_C-\phi_{\Delta C})-\frac{1}{6}i_{c1}\sin(\phi_C+\phi_{\Delta C}), \tag{6a}$$

$$\frac{d\phi_{\Delta C}}{dt}=-\frac{1}{3}i_A\sin(\phi_A)-\frac{1}{3}i_B\sin(2\phi_{\Delta C}-\phi_A)+\frac{1}{6}i_{c2}\sin(\phi_C-\phi_{\Delta C})-\frac{1}{6}i_{c1}\sin(\phi_C+\phi_{\Delta C}), \tag{6b}$$

$$\frac{d\phi_C}{dt}=1-\frac{1}{2}i_{c2}\sin(\phi_C-\phi_{\Delta C})-\frac{1}{2}i_{c1}\sin(\phi_C+\phi_{\Delta C}). \tag{6c}$$

Equations (6a)–(6c) are in final form. The impetus behind coordinate transformation (5) has to do with the question of synchronization. Since we are interested in understanding whether the radial junctions ϕ_{c1},ϕ_{c2} remain synchronized when disorder is present, the phase difference $\phi_{\Delta C}=(\phi_{c1}-\phi_{c2})/2$ is the natural variable to monitor. In particular, when this phase difference remains bounded in time, the plaquette is synchronized; if $\phi_{\Delta C}$ grows in time, synchronization is lost.

To analyze our model, we employ a variation of a multiple-time-scale perturbation scheme (see Ref. 16 for a description of the basic method). We will work in the high-bias-current regime, so that the rescaled critical currents (3) may now be regarded as small. We make this explicit by letting ϵ denote a dimensionless small parameter and writing

$$i_{c1}\to\epsilon i_{c1},\quad i_{c2}\to\epsilon i_{c2},\quad i_A\to\epsilon^2 i_A,\quad i_B\to\epsilon^2 i_B. \tag{7}$$

Note here that we use different scaling factors for the various critical currents. This is motivated by our desire to capture the transition from synchronized to desynchronized behavior in the array, which only occurs if there is sufficient variation in the critical currents. (Recall that for weak disorder, the array remains locked in a synchronized state.) Hence, if identical scaling factors had been used in Eq. (7), one would have found that the disorder would never have been large enough to force the system out of a synchronized state. In effect then, by choosing different scaling factors in Eq. (7), we are able to describe a wider range of behaviors in the array than would otherwise have been possible. (This situation is not unusual; it is well known from general asymptotic theory that a judicious choice of scaling factors often provides the key to understanding a system's behavior.) The choice of scalings in Eq. (7) can also be justified by physical arguments, since the radial and azimuthal junctions in a circular array play very different roles (this point will be discussed in more detail later).

We next introduce fast, slow, and superslow time scales $t_0=t$, $t_1=\epsilon t$, $t_2=\epsilon^2 t$ such that

$$\frac{d}{dt}=\partial_{t_0}+\epsilon\partial_{t1}+\epsilon^2\partial_{t_2} \tag{8}$$

and expand the phases

$$\phi_A=\phi_{A0}+\epsilon\phi_{A1}+\epsilon\phi_{A2}, \tag{9a}$$

$$\phi_{\Delta C}=\phi_{\Delta C0}+\epsilon\phi_{\Delta C1}+\epsilon^2\phi_{\Delta C2}, \tag{9b}$$

$$\phi_C=(\omega_0 t_0+\omega_1 t_1+\omega_2 t_2)+\phi_{C0}+\epsilon\phi_{C1}+\epsilon^2\phi_{C2}. \tag{9c}$$

Note that in the expansion for ϕ_C we have explicitly included a linear growth term $(\omega_0 t_0+\omega_1 t_1+\omega_2 t_2)$. This is because, unlike the other phase variables, we expect ϕ_C to grow approximately linearly with time [see Eq. (5) and Fig. 2(a)].

The general procedure is now as follows: We substitute Eqs. (7), (8), (9a)–(9c) into Eqs. (6a)–(6c) and collect like powers of ϵ. In this manner we obtain an entire hierarchy of equations. From these we extract so-called ''nonresonance conditions,'' which serve to suppress terms which might otherwise grow without bound and destroy the validity of our asymptotic expansion (see Ref. 16). We now carry out this procedure. (Since these calculations are somewhat lengthy, we present only the key landmarks in this construction.)

At leading order in the expansion we find

$$\partial_{t_0}\phi_{A0}=0;\quad \partial_{t_0}\phi_{\Delta C0}=0;\quad \partial_{t_0}\phi_{C0}=1-\omega_0. \tag{10}$$

The nonresonance condition associated with the third equation implies $\omega_0=1$. Solving Eq. (10) yields

$$\phi_{A0}=\phi_{A0}(t_1,t_2),\quad \phi_{\Delta C0}=\phi_{\Delta C0}(t_1,t_2),$$

$$\phi_{C0}=\phi_{C0}(t_1,t_2), \tag{11}$$

indicating that the $\phi_{A0},\phi_{\Delta C0},\phi_{C0}$ do not evolve on the fast time scale t_0.

At $\mathcal{O}(\epsilon)$, the resulting equations are

$$\partial_{t_0}\phi_{A1} = -\partial_{t_1}\phi_{A0} - \frac{1}{6} i_{c_1} \sin(t_0 + \omega_1 t_1 + \omega_2 t_2 + \phi_{C0} + \phi_{\Delta C0}) + \frac{1}{6} i_{c_2} \sin(t_0 + \omega_1 t_1 + \omega_2 t_2 + \phi_{C0} - \phi_{\Delta C0}), \quad (12a)$$

$$\partial_{t_0}\phi_{\Delta C1} = -\partial_{t_1}\phi_{\Delta C0} - \frac{1}{6} i_{c_1} \sin(t_0 + \omega_1 t_1 + \omega_2 t_2 + \phi_{C0} + \phi_{\Delta C0}) + \frac{1}{6} i_{c_2} \sin(t_0 + \omega_1 t_1 + \omega_2 t_2 + \phi_{C0} - \phi_{\Delta C0}), \quad (12b)$$

$$\partial_{t_0}\phi_{C1} = -\omega_1 - \partial_{t_1}\phi_{C0} - \frac{1}{2} i_{c_1} \sin(t_0 + \omega_1 t_1 + \omega_2 t_2 + \phi_{C0} + \phi_{\Delta C0}) - \frac{1}{2} i_{c_2} \sin(t_0 + \omega_1 t_1 + \omega_2 t_2 + \phi_{C0} - \phi_{\Delta C0}). \quad (12c)$$

The nonresonance conditions are readily extracted and solved:

$$\partial_{t_1}\phi_{A0} = 0 \rightarrow \phi_{A0} = \phi_{A0}(t_2), \quad (13a)$$

$$\partial_{t_1}\phi_{\Delta C0} = 0 \rightarrow \phi_{\Delta C0} = \phi_{\Delta C0}(t_2), \quad (13b)$$

$$\omega_1 + \partial_{t_1}\phi_{C0} = 0 \rightarrow \phi_{C0} = -\omega_1 t_1 + \hat{\phi}_{C0}(t_2). \quad (13c)$$

Solving Eqs. (12a)–(12c) yields

$$\phi_{A1} = \frac{1}{6} i_{c1} \cos(t_0 + \omega_2 t_2 + \hat{\phi}_{C0} + \phi_{\Delta C0}) - \frac{1}{6} i_{c2} \cos(t_0 + \omega_2 t_2 + \hat{\phi}_{C0} - \phi_{\Delta C0}), \quad (14a)$$

$$\phi_{\Delta C1} = \frac{1}{6} i_{c1} \cos(t_0 + \omega_2 t_2 + \hat{\phi}_{C0} + \phi_{\Delta C0}) - \frac{1}{6} i_{c2} \cos(t_0 + \omega_2 t_2 + \hat{\phi}_{C0} - \phi_{\Delta C0}), \quad (14b)$$

$$\phi_{C1} = \frac{1}{2} i_{c1} \cos(t_0 + \omega_2 t_2 + \hat{\phi}_{C0} + \phi_{\Delta C0}) + \frac{1}{2} i_{c2} \cos(t_0 + \omega_2 t_2 + \hat{\phi}_{C0} - \phi_{\Delta C0}). \quad (14c)$$

Lastly, at $\mathcal{O}(\epsilon^2)$, the nonresonant conditions are

$$\partial_{t_2}\phi_{A0} = \frac{1}{18}(i_{c2}^2 - i_{c1}^2) - \frac{5}{6} i_A \sin(\phi_{A0}) + \frac{1}{6} i_B \sin(2\phi_{\Delta C0} - \phi_{A0}), \quad (15a)$$

$$\partial_{t_2}\phi_{\Delta C0} = \frac{1}{18}(i_{c2}^2 - i_{c1}^2) - \frac{1}{3} i_A \sin(\phi_{A0}) - \frac{1}{3} i_B \sin(2\phi_{\Delta C0} - \phi_{A0}), \quad (15b)$$

$$\partial_{t_2}\hat{\phi}_{C0} = -\left(\omega_2 + \frac{1}{6}(i_{c1}^2 + i_{c2}^2)\right) - \frac{1}{6} i_{c1} i_{c2} \cos(2\phi_{\Delta C0}). \quad (15c)$$

Equations (15a)–(15c) represent the desired equations describing the basic behavior of the plaquette.

Observe that the first two equations (15a),(15b) decouple from the third, and are readily analyzed. When the disorder is small, there exist four fixed points in the $(\phi_{A0}, \phi_{\Delta C0})$ phase plane: one sink, one source, and two saddles. The system will be attracted to the sink. Accordingly, $\phi_{\Delta C0}$, which measures the phase difference between the junctions ϕ_{c1} and ϕ_{c2} [Eq. (5)], will not grow. This corresponds to the plaquette being in a synchronized state.

If the level of disorder is increased, one finds that the four fixed points approach one another in the phase plane. There is a critical level of disorder at which these fixed points simultaneously collide with one another and annihilate (in a ''double saddle-node'' bifurcation). Above this critical threshold, no fixed points exist, and the phase difference between ϕ_{c1} and ϕ_{c2} begins to grow without bound, indicating that the system has entered a desynchronized state. The precise bifurcation point can be determined via a linear stability analysis of Eqs. (15a),(15b). We find

$$\left| \frac{1}{12} \frac{(i_{c1}^2 - i_{c2}^2)}{\min(i_A, i_B)} \right| = 1, \quad (16)$$

where $\min(i_A, i_B)$ denotes the lesser of i_A, i_B. Converting back to our original parameters [see Eq. (3)], the transition boundary separating synchronized from desynchronized behavior is given by

$$\left| \frac{1}{6} \frac{(I_{c1}^2 - I_{c2}^2)}{I \min(I_{a1} + I_{a2}, I_{b1} + I_{b2})} \right| = 1. \quad (17)$$

[When the left-hand side of Eq. (17) exceeds unity, synchronization is lost.]

Equation (17) provides a quantitative prediction for the maximum amount of disorder the circular plaquette can tolerate before frequency locking is lost. The only assumption made in our derivation is that the array is operated in the high-bias-current regime ($I \gg I_{c1}, I_{c2}, I_{a1}, I_{a2}, I_{b1}, I_{b2}$). We tested our theoretical prediction against numerical simulations by fixing the values of $I_{a1}, I_{a2}, I_{b1}, I_{b2}, I$ and sweeping through different values of the critical currents I_{c1}, I_{c2}. In this manner, we numerically constructed the boundary in the $I_{c1} - I_{c2}$ parameter plane separating synchronized from desynchronized states. These results are illustrated in Fig. 5. As this shows, the agreement between our numerical results and the predictions of Eq. (17) is excellent. We remark that this agreement remains relatively good even if the bias current I is reduced so that we are no longer inside the (high-bias current) regime where the asymptotic analysis is formally valid (see, e.g., the transition point in Fig. 4).

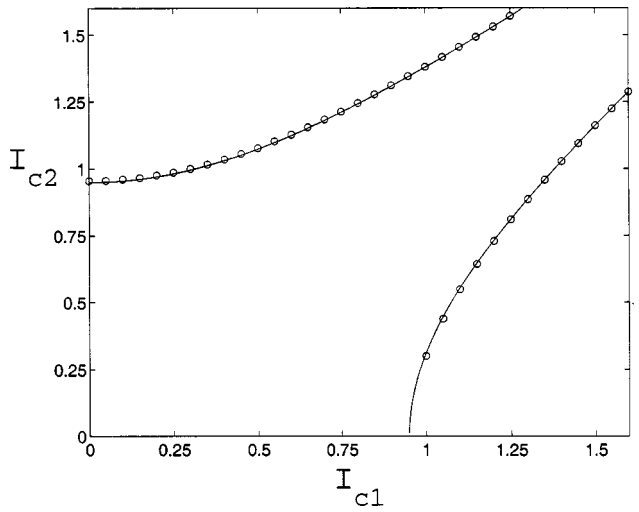

FIG. 5. The transition boundary separating sychronized from desynchronized behavior. Synchronized states lie in the interior region between the upper and lower curves. This plot was constructed by fixing $I=9$, $I_{a1}=0.0056$, $I_{a2}=0.0111$, $I_{b1}=0.30$, $I_{b2}=0.07$ and sweeping through the $I_{c1}-I_{c2}$ parameter plane to locate transition points. The circles mark the numerically determined transition points, while the solid curves represent the theoretical boundaries predicted by the transition formula (17).

The transition formula (17) reveals that the plaquette is robust against even very high levels of disorder. For example, variations as large as 50% in the values of the critical currents from one junction to the next are not sufficient to desynchronize the array (with present fabrication techniques, the typical size of variations can be reduced to about the 1% level). In this respect, then, the circular geometry of the plaquette is intrinsically good at fostering coherent oscillations among the individual junctions even in the presence of relatively high levels of disorder. The quantification of this result in the form of Eq. (17) represents a key result of our asymptotic analysis.

Moreover, the mathematical analysis leading to Eq. (17) also uncovers the principal physical mechanism responsible for the onset of desynchronized behavior for sufficiently high levels of disorder. A stability analysis reveals that the bifurcation described above in which the four fixed points collide and annihilate in the $(\phi_{A0},\phi_{\Delta C0})$ phase plane occurs precisely when either $|\sin(\phi_{A0})|$ or $|\sin(2\phi_{\Delta C0}-\phi_{A0})|$ equals unity. Now, the variable ϕ_{A0} represents the phase of the outer two azimuthal junctions of the circular plaquette, while $(2\phi_{\Delta C0}-\phi_{A0})$ represents the phase of the inner two azimuthal junctions [this may be seen by tracing back the sequence of transformations that led from Eqs. (1a)–(1f) to Eqs. (15a)–(15c)]. Therefore, the quantities $|\sin(\phi_{A0})|$, $|\sin(2\phi_{\Delta C0}-\phi_{A0})|$ above are simply proportional to the amount of supercurrent passing through the outer and inner azimuthal junctions, respectively. Hence, the meaning of the conditions $|\sin(\cdots)|=1$ is that the amount of supercurrent being passed by any of the azimuthal junctions has attained its maximum allowed value. In other words, *synchronization is lost when the supercurrent passing through any azimuthal junction equals the critical current of that junction.* This is the fundamental physical mechanism behind the loss of synchronization in a circular plaquette subject to strong disorder.

IV. COMPARISON TO RECTANGULAR PLAQUETTE AND GENERALIZATIONS TO LARGER ARRAYS

Despite some distinctions (to be discussed shortly), the similarities between the circular plaquette model described here and previous analytical studies of a rectangular plaquette model[14,15] are both striking and informative. First, we observe that for both geometries, the arrays are able to tolerate disorder and remain synchronized, provided the disorder lies below a critical threshold level. Second, and much more revealing, we now know (based on the analysis in Sec. III) that the mechanism by which disorder destroys synchronization in a Josephson plaquette with circular geometry is *identical* to that found in a plaquette with rectangular geometry (see Ref. 14): Synchronization is lost when the supercurrent through the azimuthal junctions reaches its maximum allowed value. (Note: the ''horizontal'' junctions of the rectangular plaquette play the role of the ''azimuthal'' junctions in the circular plaquette.) The implications of this are significant: This finding suggests that perhaps the principal mechanism underlying disorder-induced desynchronization in a Josephson junction array is universal, i.e., independent of the underlying lattice geometry. (We must emphasize, however, that this suggestion is only speculative at present—we can claim rigorous results only for the case of plaquettes with circular and rectangular geometries. Moreover, the precise manner in which bias current is fed into an array most likely plays a role here as well, but this issue has yet to be fully explored.)

It is important to note that while the mechanism by which disorder destroys synchronization may be the same for both the circular and rectangular cases, this does not mean that these two arrays are identical in terms of their ability to tolerate disorder. Indeed, a comparison of the transition formula (17) with the corresponding transition formula for the rectangular-geometry case (see Ref. 14) reveals that the circular plaquette is the more robust of the two against disorder (although only modestly more so). This ability to tolerate higher levels of disorder comes at a price, however, six Josephson junctions are required to construct the circular plaquette, but only four are needed in the rectangular case.

Lastly, we speculate as to what might occur if we consider generalizations of our circular plaquette (which is a 2×2 circular array) to larger $(N\times M)$ circular arrays. Are the synchronization properties of larger circular arrays similar to that of the plaquette, or might new features arise? This question is especially intriguing in light of what has been learned recently about generalizations of the rectangular plaquette model (a 2×2 array) to larger $(N\times M)$ rectangular arrays. In particular, if an $N\times M$ rectangular Josephson junction array (with $N>2$) is subjected to weak levels of disorder, the array only partially synchronizes: The junctions across any given row of the array all synchronize with one another, but there is no synchronization from one row to the next.[9,17,14] In other words, the synchronization mechanism observed in an isolated rectangular plaquette operates across rows in larger arrays, but not between rows. Ultimately, this failure to fully synchronize traces its origins to a highly unusual mathematical property possessed by $N\times M$ rectangular arrays in the absence of disorder: *neutral stability*.[18,19,15] In this context, neutral stability refers to the fact that it is possible to perturb

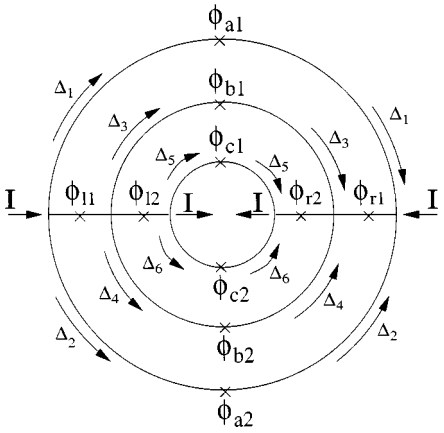

FIG. 6. *A* 3×2 *circular array*. $\phi_{l1},\phi_{r1},\phi_{l2},\phi_{r2}$ denote the four radial junctions, and $\phi_{a1},\phi_{a2},\phi_{b1},\phi_{b2},\phi_{c1},\phi_{c2}$ the six azimuthal junctions. An externally imposed bias current I is fed into and extracted from the array as shown. $\Delta_1,\Delta_2,\Delta_3,\Delta_4,\Delta_5,\Delta_6$ represent the spontaneously induced shunt currents in the array.

the junctions within any given row of a rectangular array in such a manner that the system has no natural tendency to return to its original (preperturbed) configuration (see Ref. 18). [Indeed, it was the discovery of neutral stability and related nongeneric mathematical properties (e.g., Ref. 20) that originally stimulated a great deal of interest in Josephson junction arrays among the nonlinear dynamics community.]

Hence, to understand the behavior of large circular arrays, a natural starting point is to first ask if $N\times M$ circular arrays ($N>2$) also possess the neutral-stability property. If so, one might reasonably speculate that such arrays will exhibit only partial synchronization when subjected to weak disorder, i.e., if one pictures the radial junctions in a circular array as forming a series of concentric rings, then the radial junctions within any given ring should synchronize, but no synchronization would be expected as one moves radially inward from one ring to the next.

We offer here a preliminary inquiry into this issue by considering the 3×2 circular array depicted in Fig. 6. The equations of motion are constructed in the usual manner. We find

$$\frac{\hbar}{2er}\dot{\phi}_{l1}+I_{l1}\sin(\phi_{l1})=I-\Delta_1-\Delta_2, \tag{18a}$$

$$\frac{\hbar}{2er}\dot{\phi}_{r1}+I_{r1}\sin(\phi_{r1})=I+\Delta_1+\Delta_2, \tag{18b}$$

$$\frac{\hbar}{2er}\dot{\phi}_{l2}+I_{l2}\sin(\phi_{l2})=I-\Delta_1-\Delta_2-\Delta_3-\Delta_4, \tag{18c}$$

$$\frac{\hbar}{2er}\dot{\phi}_{r2}+I_{r2}\sin(\phi_{r2})=I+\Delta_1+\Delta_2+\Delta_3+\Delta_4, \tag{18d}$$

$$\frac{\hbar}{2er}\dot{\phi}_{a1}+I_{a1}\sin(\phi_{a1})=\Delta_1, \tag{18e}$$

$$\frac{\hbar}{2er}\dot{\phi}_{b1}+I_{b1}\sin(\phi_{b1})=\Delta_3, \tag{18f}$$

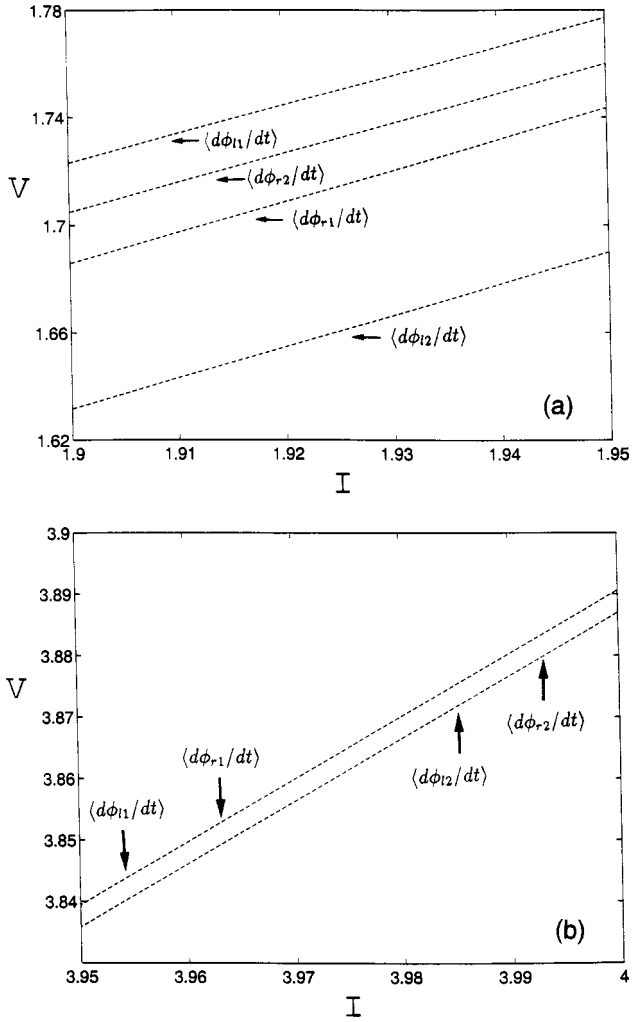

FIG. 7. *I-V* plot for the 3×2 circular array. The time-averaged voltage across each radial junction $\langle d\phi_{l1}/dt\rangle$, $\langle d\phi_{r1}/dt\rangle$, $\langle d\phi_{l2}/dt\rangle$, $\langle d\phi_{r2}/dt\rangle$ as a function of imposed current I is shown. The critical currents were held fixed at $I_{l1}=0.3$, $I_{r1}=1.5$, $I_{l2}=1.6$, $I_{r2}=0.2$, $I_{a1}=0.06$, $I_{a2}=0.11$, $I_{b1}=0.4$, $I_{b2}=0.2$, $I_{c1}=0.1$, $I_{c2}=0.04$. (a) for low values of the bias current, all four junctions are desynchronized. (b) at higher bias current, the outer junctions ϕ_{l1}, ϕ_{r1} become frequency locked, as do the inner junctions ϕ_{l2}, ϕ_{r2}. Observe, however, that the outer and inner pairs are not synchronized, owing to the neutral stability property of the 3×2 array.

$$\frac{\hbar}{2er}\dot{\phi}_{c1}+I_{c1}\sin(\phi_{c1})=\Delta_5, \tag{18g}$$

$$\frac{\hbar}{2er}\dot{\phi}_{a2}+I_{a2}\sin(\phi_{a2})=\Delta_2, \tag{18h}$$

$$\frac{\hbar}{2er}\dot{\phi}_{b2}+I_{b2}\sin(\phi_{b2})=\Delta_4, \tag{18i}$$

$$\frac{\hbar}{2er}\dot{\phi}_{c2}+I_{c2}\sin(\phi_{c2})=\Delta_6, \tag{18j}$$

together with constraint relations

$$\phi_{a1}-\phi_{a2}=0,\quad \phi_{b1}-\phi_{b2}=0,\quad \phi_{c1}-\phi_{c2}=0, \tag{19a}$$

$$\phi_{a1}+\phi_{r1}-\phi_{b1}-\phi_{l1}=0, \quad \phi_{b1}+\phi_{r2}-\phi_{c1}-\phi_{l2}=0, \tag{19b}$$

$$\Delta_1+\Delta_2+\Delta_3+\Delta_4+\Delta_5+\Delta_6=0. \tag{19c}$$

Owing to the presence of the constraints, Eqs. (18a)–(18j) may be reduced down to a five-dimensional dynamical system. These calculations are lengthy and we do not reproduce them here.

Observe that if we set all the critical currents in Eqs. (18a)–(18j) the same (i.e., the zero-disorder case), then there exists an ''in-phase'' solution of the form $\phi_{l1}=\phi_{r1}=\phi_{l2}=\phi_{r2}=\phi(t)$, with all the azimuthal junctions identically zero. Now, a straightforward check reveals that $\phi_{l1}=\phi_{r1}=\phi(t)$, $\phi_{l2}=\phi_{r2}=\phi(t+\delta)$ is also a solution of these equations (with δ an arbitrary constant), indicating that this circular array does indeed possess the neutral stability property found previously in a rectangular array (see Refs. 18 and 15 for a more general discussion).

This result is both significant and (from a mathematical perspective) somewhat surprising. It is significant because it suggests that indeed the circular array might exhibit only partial synchronization when weak disorder is present. It is surprising because neutral stability is a nongeneric mathematical property that in general would not be expected to persist if one makes changes to a system, and yet it has survived the change from a rectangular to circular lattice geometry. We do not yet have a complete understanding of why this should be the case.

To verify our hypothesis about partial synchronization in a 3×2 circular array, we ran a series of numerical simulations. The resulting *I*-*V* diagram is shown in Fig. 7. We find that for low values of the bias current, all four radial junctions ϕ_{l1}, ϕ_{r1}, ϕ_{l2}, ϕ_{r2} are desynchronized [Fig. 7(a)]. As the bias current is increased, the outer junctions ϕ_{l1}, ϕ_{r1} eventually synchronize with one another [as in the plaquette case (Fig. 4)]. Likewise, the inner pair ϕ_{l2}, ϕ_{r2} also eventually synchronizes (though not at the same time as the outer pair). Observe, however, that the outer and inner pairs of junctions do not synchronize with one another, see Fig. 7(b).

V. CONCLUSIONS

In this paper we have presented a detailed analytical description of the behavior of a 2×2 Josephson junction array with a circular geometry, culminating in a quantitative assessment of its ability to remain synchronized in the presence of disorder. The primary physical mechanism responsible for the loss of synchronization when disorder becomes too large has also been identified, and has been shown to be identical to that found previously in a 2×2 rectangular array. This finding suggests that the underlying cause of disorder-induced desynchronization in an array might be more general than previously believed, and transcend the particular lattice geometry of the array.

Moreover, our study of the circular plaquette indicates that larger circular arrays can also synchronize when disorder is present (provided the disorder is not too large), but that this synchronization is only partial, owing to the (somewhat surprising) existence of the neutral stability property in these larger arrays. Thus, in terms of the *intrinsic* ability of lattice geometry to promote synchronization, we have determined that a *circular* lattice geometry is only partially successful in this regard (i.e., the circular geometry does not naturally induce synchronization in the radial direction, though it does in the azimuthal direction). Hence, while it may still be possible to fully synchronize a circular array by other means (e.g., by applying a high-frequency external signal, coupling the array to an external load, or through nonlocal mutual inductance effects, etc.), the innate contribution of the (circular) lattice structure to the synchronization process has been demonstrated to be somewhat limited. It remains to be seen whether other lattice geometries might exist that are intrinsically better at promoting (full) synchronization in an array compared to the circular or rectangular cases.

[1] D. R. Tilley, Phys. Lett. **33A**, 205 (1970).
[2] K. K. Likharev, *Dynamics of Josephson Junctions and Circuits* (Gordon and Breach, New York, 1986).
[3] T. D. Clark, Phys. Rev. B **8**, 137 (1973).
[4] A. K. Jain, K. K. Likharev, J. E. Lukens, and J. E. Savageau, Phys. Rep. **109**, 309 (1984).
[5] M. Darula, T. Doderer, and S. Beuven, Supercond. Sci. Technol. **12**, R1 (1999).
[6] P. Hadley, M. R. Beasley, and K. Wiesenfeld, Phys. Rev. B **38**, 8712 (1988).
[7] G. Filatrella and K. Wiesenfeld, J. Appl. Phys. **78**, 1878 (1995).
[8] B. Larsen and S. P. Benz, Appl. Phys. Lett. **66**, 3209 (1995).
[9] S. P. Benz and C. J. Burroughs, Appl. Phys. Lett. **58**, 2162 (1991).
[10] M. Octavio, C. B. Whan, and C. J. Lobb, Appl. Phys. Lett. **60**, 766 (1990).
[11] M. Darula, P. Seidel, J. von Zameck Glyscinski, A. Darulova, F. Busse, and S. Benacka, in *Applied Superconductivity*, edited by H. C. Freyhardt (DGM Informationsgesellschaft, Oberursel, 1993), p. 1245.
[12] P. A. A. Booi and S. P. Benz, Appl. Phys. Lett. **64**, 2163 (1994).
[13] R. L. Kautz, IEEE Trans. Appl. Supercond. **5**, 2702 (1995).
[14] A. S. Landsberg, Y. Braiman, and K. Wiesenfeld, Appl. Phys. Lett. **67**, 1935 (1995).
[15] A. S. Landsberg, Y. Braiman, and K. Wiesenfeld, Phys. Rev. B **52**, 15 458 (1996).
[16] A. H. Nayfeh, *Introduction to Perturbation Methods* (Wiley, New York, 1981).
[17] C. B. Whan *et al.*, Bull. Am. Phys. Soc. **40**, 117 (1995).
[18] K. Wiesenfeld, S. P. Benz, and P. A. A. Booi, J. Appl. Phys. **76**, 3835 (1994).
[19] P. Hadley, Ph.D. thesis, Stanford University, 1989.
[20] S. Watanabe and S. H. Strogatz, Physica D **74**, 197 (1994).